Experimental Study of Unconfined and Confined Isothermal Swirling Jets

Rohit Sharma, Fabio Cozzi

Abstract—A 3C-2D PIV technique was applied to investigate the swirling flow generated by an axial plus tangential type swirl generator. This work is focused on the near-exit region of an isothermal swirling jet to characterize the effect of swirl on the flow field and to identify the large coherent structures both in unconfined and confined conditions for geometrical swirl number, $S_g = 4.6$. Effects of the Reynolds number on the flow structure were also studied. The experimental results show significant effects of the confinement on the mean velocity fields and its fluctuations. The size of the recirculation zone was significantly enlarged upon confinement compared to the free swirling jet. Increasing in the Reynolds number further enhanced the recirculation zone. The frequency characteristics have been measured with a capacitive microphone which indicates the presence of periodic oscillation related to the existence of precessing vortex core, PVC. Proper orthogonal decomposition of the jet velocity field was carried out, enabling the identification of coherent structures. The time coefficients of the first two most energetic POD modes were used to reconstruct the phase-averaged velocity field of the oscillatory motion in the swirling flow. The instantaneous minima of negative swirl strength values calculated from the instantaneous velocity field revealed the presence of two helical structures located in the inner and outer shear layers and this structure fade out at an axial location of approximately $z/D = 1.5$ for unconfined case and $z/D = 1.2$ for confined case. By phase averaging the instantaneous swirling strength maps, the 3D helical vortex structure was reconstructed.

Keywords—Acoustic probes, 3C-2D particle image velocimetry, PIV, precessing vortex core, PVC, recirculation zone.

I. INTRODUCTION

SWIRLING jets are widely used in several industrial applications [1]. For example in gas turbines combustors and burners, the swirling flow is used to enhance mixing in combustion chambers to improve flame stabilization, air/fuel mixing and pollutant emissions. Swirling jets have been profoundly investigated throughout the last decades. Despite such comprehensive studies, they still remain a subject of interest in both academia and industry because the rich variety of phenomenon they show, such as recirculation, vortex breakdown, PVC and the instability associated with it, is still not fully understood. The behavior of swirling jets is known to

depend strongly on swirl intensity, the latter is quantified by a non-dimensional parameter named swirl number, S, that compares tangential to axial velocities. The most common definition of the swirl number is based on the ratio of the axial flux of angular momentum, G_θ to the axial flux of axial momentum, G_z times a nozzle radius, R, i.e. $S = \frac{G_\theta}{G_z R}$. Experimental studies evidence an abrupt change in the flow structure when the swirl number is above a critical value, $S_{cr} \sim 0.6$ [1]; specifically it is observed an abrupt deceleration of the fluid on the swirling jet axis leading to the formation of a stagnation point followed by a region of reversed flow [1]-[3]. This phenomenon is called vortex breakdown (VB). Another well-known instability is relevant to swirling flows; the so-called PVC which is periodic in nature and it is usually associated with the VB and the existence of a central recirculation zone. Jet precession is also known to occur even in low swirling jets [4]. Despite the related number of experimental, theoretical and numerical studies the VB and the PVC phenomena are still not fully understood [2], [5]-[7].

The effect of confinement has a remarkably significant effect upon the VB and its related instabilities. The formation of a reverse flow zone primarily depends on the swirl intensity and downstream confinement and therefore has particular implications regarding the sub-critical nature of the flow and the formation of hydrodynamic instability [2], [8]. Confinement ratio, D_o/D_e, is the dominant factor, where D_o = diameter of confinement and D_e = diameter of nozzle exit, the smaller this ratio the larger is the effect. Khalil et al. [9] experimentally investigated the impact of confinement on swirl assisted combustion with focus on the flow field under unconfined and confined conditions. The features of the flow field were characterized under both isothermal and reacting conditions. For this swirler, the contraction ratio was 0.3636. The swirl burner was confined using a quartz cylinder with a diameter ratio (D_q/D_b) of 1.7, where D_q is the quartz diameter and D_b is the burner diameter, leading to an area ratio of 2.9. Results exhibited the traditional central toroidal recirculation zone (CTRZ) for the unconfined cases whereas this zone shortened and widened with increased RMS fluctuations upon confinement. CTRZ further enhanced and the magnitude of velocity and turbulence is increased upon the increase in Reynolds number [9]. Ceglia et al. [10] showed that the swirl number increases due to confinement and spreading of the swirling jet is larger; further enhance the turbulence intensity at the nozzle exit.

Experimental techniques of the last decades such as PIV or LDV associated with data treatment able to extract the coherent structure embedded in the flow or either the

R.Sharma is with the Energy Department, Politecnico di Milano, Via Lambruschini 4, Milano 20156 Italy (phone: +39-02-23993909; fax: +39-02-23993913; e-mail: rohit.sharma@polimi.it).

F.Cozzi is with the Energy Department, Politecnico di Milano, Via Lambruschini 4, Milano 20156 Italy (phone: +39-02-23998616; fax: +39-02-23993913; e-mail: fabio.cozzi@polimi.it).

World Academy of Science, Engineering and Technology
International Journal of Mechanical and Mechatronics Engineering
Vol:11, No:2, 2017

amplitude of the periodic velocity fluctuations have grown in popularity and have been applied to many different complex flow, for e.g. flow in cylinder wakes [11], [12], swirling flow [13], [14] and in-cylinder engine flows [15]. Combination of PIV measurements with Proper orthogonal decomposition (POD) analysis was found to be very powerful tool in identifying the coherent structures. POD technique is one of the data analysis technique often used for such analysis. Lumley et al. [16] is generally attributed as being the first to suggest POD application. Oberleithner et al. [13] reconstructed the 3D periodic swirling flow from PIV snapshots using POD and phase averaging method. They claimed that the POD approach yielding a more accurate result as compared to single point time resolved LDA measurement because POD approach measured the phase angle from spatial modes. In the case of periodic oscillation, a special feature of POD is its ability to determine the phase with respect to the periodic cycle proposed by Oudheusden et al. [12], Stohr et al. [14]. They used the first two POD coefficients as the global phase indicator which allows the estimation of conditional phase averaging. Stohr et al. [14] found that the small scale structures are represented more accurately in the phase averages than in the low-order POD reconstructed flow.

The purpose of the present paper is to analyze the effects of confinement and Reynolds number on the flow structure generated by axial plus tangential entry swirl generator and to investigate the 3D helical vortex structure emerging in the unconfined and confined isothermal turbulent swirling jets associated with the VB and PVC through the combination of Stereo-PIV measurements and POD analysis. A detailed analysis of the influence of swirl intensity on central recirculation zone, VB, and precession frequencies has been reported in the work of Cozzi et al. [17]. Extending this work, POD is applied in both unconfined and confined swirling jets PIV data in longitudinal plane to characterize the effect of the influence on the fluctuating flow. In the POD based analysis the PVC come into sight in each sector as a pair of eigenmodes. POD time coefficient method used for phase identification and thereby phase averages of instantaneous flow field are calculated to capture the organized vortical structures.

II. EXPERIMENTAL SET-UP AND DATA ANALYSIS

A. Experimental Apparatus

A vertically mounted swirl generator was used to generate isothermal swirling air jets as shown in Fig. 1. The swirl generator consists of a pipe of 80 mm in diameter and about 180 mm in length, it is followed by a converging section of 160 mm length, at the end of the converging section is located a cylindrical nozzle of 40 mm in length and internal diameter D=36 mm. The axial-plus-tangential entry type swirl burner allows varying the intensity of swirl by changing the axial and tangential flow rates of air by means of thermal mass flow meters with 1% accuracy. The axial air introduces through 4 radial entrances in the cylindrical chamber and to produce the uniform axial stream, it passes through a cylindrical plate with

24 holes of 2 mm diameter. The angular momentum is imparted by tangential air which is introduced through 8 tangential inlets. Finally, there is a gas gun of 8 mm inner diameter and 400 mm length, the gas gun is used only to provide the seeded air flow necessary for the PIV measurements, as such its exit section is placed to the level of the cylindrical disc, see Fig. 4. This type of insemination is advantageous because it allows to mix the two streams efficiently with the tangential air.
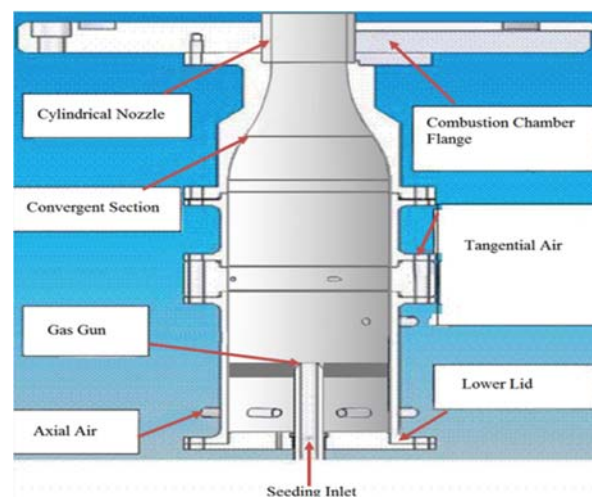

Fig.1 Schematic of the swirling burner

The combustion chamber with optical access was designed with an octagonal cross-section as shown in Fig. 2 (b) to allow an easy installation of the plane quartz windows. This cross-section encloses a circle with a diameter of 0.193 m. The size of each wall of the combustion chamber is 80 mm in width and 290 mm in height. The optical access for PIV measurements was through 2 quartz windows (80 mm * 290 mm) other 2 windows were mounted on opposite side of the chamber to let the laser beam passed through the combustion chamber. The corresponding confinement ratio is $\frac{D_o}{D}$= 5.4, where D_o = Diameter of confinement and D = Diameter of nozzle = 0.036 m.

B. Measurement techniques

3C-2D PIV was employed to measure the velocity field of the swirling jet at the nozzle exit in a longitudinal plane. The small seeding particles are illuminated using double pulse Nd:YAG laser (energy ≈ 200 mJ/pulse; λ = 532 nm) light source provided by Quanta system. Here, a laser sheet thickness of about 1.5 mm fired vertically close to the nozzle exit. The image acquisition hardware that came with the Dantec's Dynamics PIV system used in this work included two Hamamatsu C8484-05C HiSense MkII high-resolution cameras equipped with Nikon lenses with focal length, f equal to 60 mm were mounted according to the Scheimpflug rules and maximum aperture equal to 2.8. These cameras use a charge-coupled device (CCD) which is comprised of a 1344 (H) x 1024 (V) matrix suitably synchronized with the laser, so as to acquire the images in correspondence with the scatter of laser pulses off the particles. Double images were acquired at

World Academy of Science, Engineering and Technology
International Journal of Mechanical and Mechatronics Engineering
Vol:11, No:2, 2017

a rate of 5 Hz with time between pulses of the order of 10-30 μs, depending on the swirl intensity. Oil droplets with the average diameter of 1-2 μm are produced by a jet atomizer used to seed the jet flow; the seeding is injected inside the swirl generator through the central pipe (gas gun), to avoid interference with the swirling flow the gas gun exit is located about 8D below the exit plane of the nozzle. When analyzing the unconfined flow a six-jet Atomizer is also used to provide the external seeding particles, the latter are homogeneously distributed throughout the measurement plane by means of pipes arranged around the burner. The acquired images are processed using Dantec's DynamicStudio 4.15 software. The non-uniformities of laser light sheet prior to cross-correlation was corrected by using an image balancing filter with a smooth cell size of 5 x 5 on the raw images. Image interrogation was done with the adaptive cross-correlation (using FFT and iterations for offsetting the second interrogation window). The final size of interrogation zone was 32 x 32 pixels with 50% overlap of the interrogation zones and the number of refinement steps was fixed as two. Finally, the method proposed by Soloff et al. [18] and implemented in the Dantec software was used to reconstruct the third velocity component from the two 2D vectors fields. Average flow map were obtained by averaging 700 instantaneous vector fields.

The laser sheet passed through the vertical axis of the burner (meridional or longitudinal plane) for both unconfined and confined flow as shown in Figs. 2 (a), (b). The resolution in the 3C velocity maps was about 2.5×1.7 mm^2 for unconfined flow and 2.1×1.3 mm^2 for confined region.

TABLE I
FLOW CONDITIONS

|	Axial flow [Nl/min]	Axial flow insemination [Nl/min]	Tangential flow [Nl/min]	Re	S_g	S_1
Unconfined	292	8	200	21800	4.6	1.4
Confined	291	9	200	21800	4.6	3

III. METHODOLOGY AND CHARACTERIZATION PARAMETERS

The swirl intensity for rotating flows is usually characterized by the non-dimensional swirl number, given by [19]:

$$S = \frac{G_\theta}{G_z R} \qquad (1)$$

where G_θ = axial flux of angular momentum, G_z = axial flux of axial momentum, R = nozzle radius. Swirl number can be written in number of ways depending on the assumptions [1], [19]. For an incompressible isothermal flows by neglecting contribution from turbulent component and expressing the one due to pressure in terms of azimuthal velocity [20], (1) can be rewritten as:

$$S_1 = \frac{\int_0^r r^2 UW dr}{\left[\int_0^r r(U^2 - \frac{1}{2}W^2)dr\right] \times R} \qquad (2)$$

The definition of swirl number S_1 is used here to characterize the flow field where U, W and ρ are the time averaged axial velocity, time mean azimuthal velocity, and air density respectively.
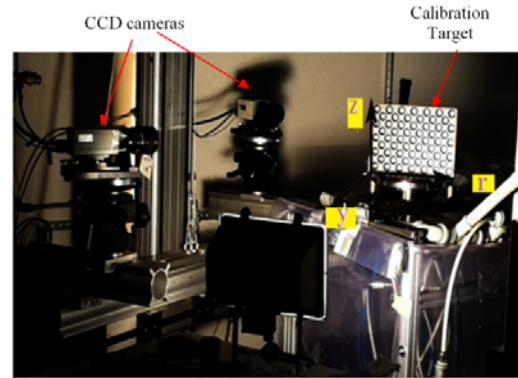
(a)
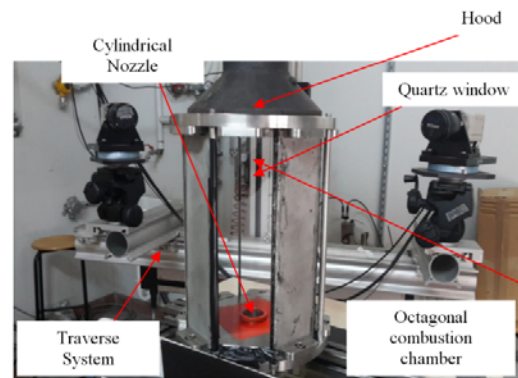
(b)

Fig. 2 Experimental set-up: camera oriented for longitudinal plane measurements (a) for unconfined flow and (b) for confined flow

With axial plus tangential swirl generator it was found by Claypole and Syred [21] that a convenient way to examine the swirl number was to use the axial and tangential mass flow rates to determine a geometric swirl number (S_g) which is given by:

$$S_g = \frac{\pi R_o R}{A_T}\left(\frac{\dot{m}_{tangential}}{\dot{m}_{tangential} + \dot{m}_{axial}}\right)^2 \qquad (3)$$

where R_o = radial distance of tangential inlets from burner axis, R = nozzle radius, A_T = total area of tangential air inlets, $\dot{m}_{tangential}$ and $\dot{m}_{axial}$ = mass flow rate of tangential and axial air inlets. This definition of swirl number being based only on geometrical quantities and mass flow rates results to be independent from the actual mean velocity profiles at the nozzle exit.

The Reynolds number, Re = $(\rho * U_{bulk} * D) / \mu$ is based on nozzle diameter, D=2R, the bulk mean velocity, U_{bulk}, and the dynamic air viscosity, μ. Flow conditions are listed in Table I.

World Academy of Science, Engineering and Technology
International Journal of Mechanical and Mechatronics Engineering
Vol:11, No:2, 2017

IV. PROPER ORTHOGONAL DECOMPOSITION

The POD method decomposes the original instantaneous velocity field into modes and their corresponding energies (or eigenvalues). It is obvious to apply the POD to velocity, since the optimization of the basis in L_2 space separates and ordering the mode according to the energy which usually associated with the large scale flow structures [22]. POD has also been used as a tool for the comparison of PIV and Large Eddy Simulation (LES) data in [30] and it is also shown that POD modes have a good qualitative agreement between PIV and LES. The method of snapshots [23] which is known to be computationally efficient is used here. Here each instantaneous velocity measurement by PIV is considered to be a snapshot of the flow. An analysis is then performed on the 700 snapshots acquired in both unconfined and confined conditions. The first step is to calculate the mean velocity field. The mean velocity field can be considered as the zeroth mode of the POD. The principal idea behind POD is to calculate a set of linear basis functions, also called POD modes, which represents the fluctuating parts of the velocity components of the flow (u_j^n, v_j^n, w_j^n) where u, v, w represents the fluctuating parts of each of the three velocity components. Index n runs through the N snapshots and j runs through the M positions of velocity vectors in a given snapshots i.e. $u_j = u(x_j, y_j, z_j)$. All fluctuating velocity components from the N snapshots arranged in a matrix A as:

$$A = [u^1 \quad u^2 \quad \cdots \quad u^N] = \begin{bmatrix} u_1^1 & u_1^2 & \cdots & u_1^N \\ \vdots & \vdots & \vdots & \vdots \\ u_M^1 & u_M^2 & \cdots & u_M^N \\ v_1^1 & v_1^2 & \vdots & v_1^N \\ \vdots & \vdots & \cdots & \vdots \\ v_M^1 & v_M^2 & \vdots & v_M^N \\ w_1^1 & w_1^2 & \cdots & w_1^N \\ \vdots & \vdots & \vdots & \vdots \\ w_M^1 & w_M^2 & \cdots & w_M^N \end{bmatrix} \quad (4)$$

The NxN auto covariance matrix C is created from the A matrix as:

$$C = A^T A \quad (5)$$

and the corresponding eigenvalue is calculated as:

$$CB_i = \lambda_i B_i \quad (6)$$

where λ_i and B_i are corresponding eigenmodes and eigenvectors. The modes are arranged such that their energies are sorted according to the size of their eigenvalues:

$$\lambda_1 > \lambda_2 > \lambda_3 > \ldots\ldots\ldots\ldots.\lambda_N = 0 \quad (7)$$

According to such sorting criteria, the periodic motion in complex flow is always represented by the first several modes. The eigenvectors corresponding to each of the eigenvalues make up a basis for constructing the eigen-functions, which are normalized to get POD modes:

$$\phi_i = \frac{AB_i}{|AB_i|}, i = 1, 2, \ldots\ldots\ldots.N-1 \quad (8)$$

where B_i is the ith eigenvector corresponding to the eigenvalue λ_i and modes are normalized by discrete 2-norm defined as:

$$\|y\| = \sqrt{y_1^2 + y_2^2 + \cdots \ldots y_M^2} \quad (9)$$

Each snapshot can be expanded in a series of the POD modes with POD coefficients a_n for each POD mode n determined by projecting the fluctuating part of the velocity field onto the POD modes:

$$a_n = \varphi^T u_n \quad (10)$$

where $\varphi = \phi_1, \phi_2 \ldots\ldots \phi_{N-1}$. The velocity part of a snapshots n reads:

$$u_n = \sum_{i=1}^{N} a_i^n \phi_i^n = \varphi a_n \quad (11)$$

The amount of total energy from velocity fluctuations associated with a given POD mode is proportional to the corresponding eigenvalue.

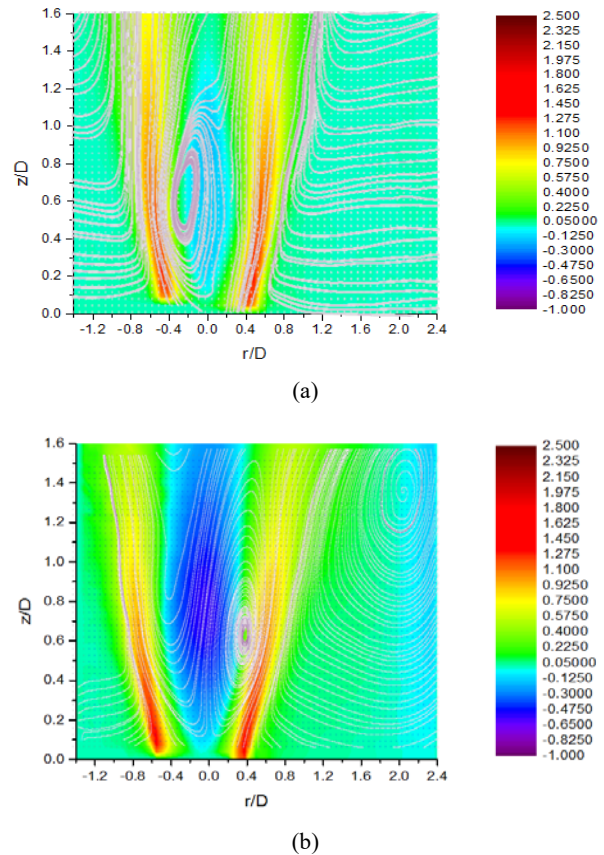## V. RESULTS AND DISCUSSION

A. Unconfined and Confined Mean Flow Field

(a)

(b)

Fig. 3 Contours and streamlines of average axial velocity for Re = 21800. (a) - Unconfined case, (b) - Confined flow

World Academy of Science, Engineering and Technology
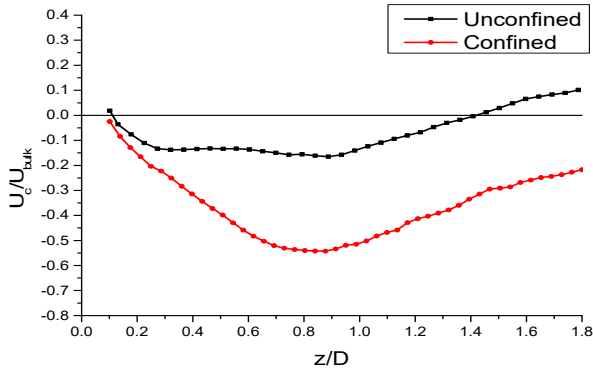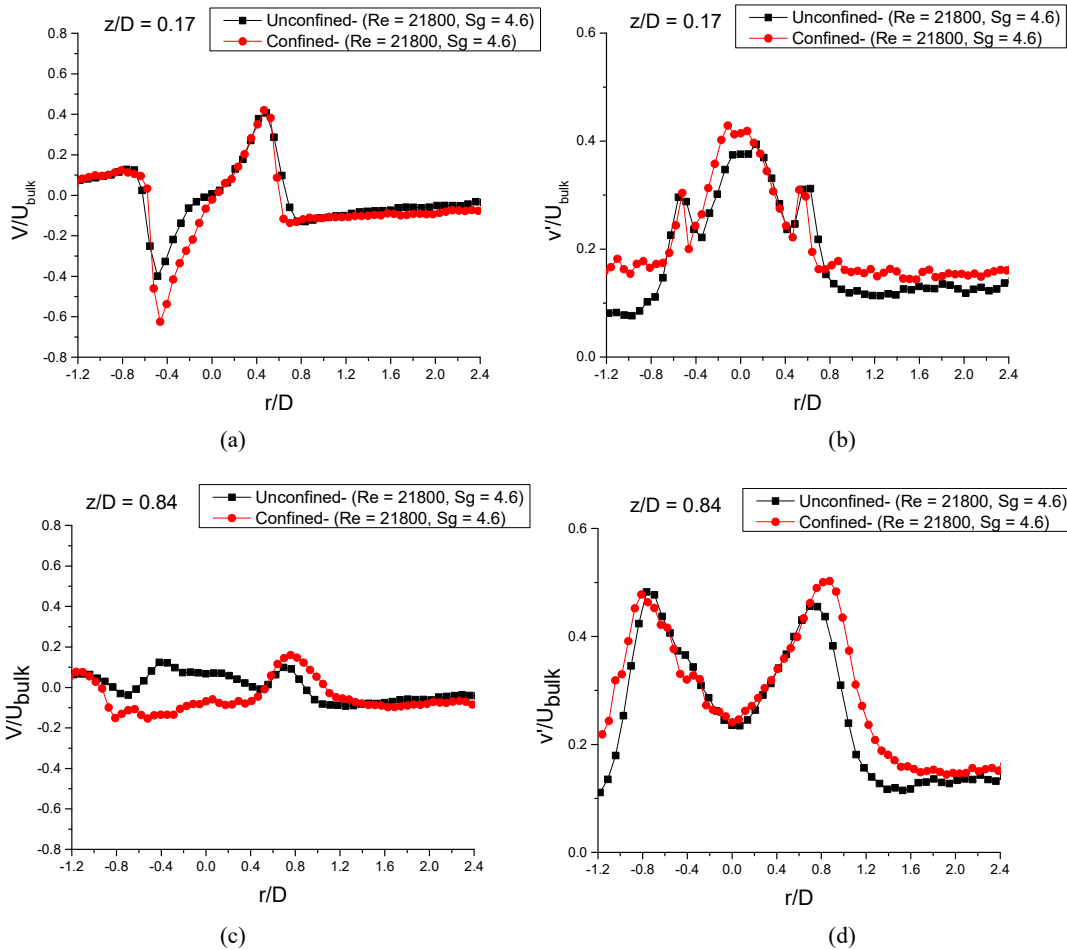International Journal of Mechanical and Mechatronics Engineering
Vol:11, No:2, 2017

Fig. 4 Centerline mean axial velocity profiles

The coordinates are normalized by the diameter of nozzle i.e. D = 36 mm and the time averaged velocity and its fluctuating components, normalized by the U_{bulk} = 8.88 m/s. In Figs. 3 (a) and (b), the velocity field of the unconfined and confined swirling jets at Reynolds number, Re = 21800 and geometrical swirl number, S_g = 4.6, is characterized by the contours of average axial velocity, U on the radial-axial plane. The streamlines are also shown on the contour to outline the flow behavior. For both unconfined and confined cases, the axial velocity contours shows a symmetrical distribution with respect to the axis of the nozzle. It presents a strong

recirculation in the central region of the jet with negative axial velocity and there is always a wake-like profile starting from the nozzle axis. These features evidence the occurrence of the VB. One can notice the recirculation zone was significantly enlarged in length and widened upon confinement. For the unconfined case, the central recirculation zone (CRZ) reached a downstream position of z/D ≅ 1.4 whereas for confined case CRZ further strengthened towards downstream.

Fig. 4 shows the length of the CRZ, which is determined by the negative average axial velocity at the centerline. The length of the CRZ for the confined case (i.e. the average axial velocity at the centerline is negative throughout the field of view) is larger than the unconfined case. Furthermore, a corner recirculation zone (CoRZ) is formed at z/D ≅ 1.4 as shown in Fig. 3 (b), between the combustion chamber wall and the outer shear layer (OSL) due to jet expansion in presence of confinement. It is worth to note that the confinement causes an increase of the swirl number as compared to unconfined swirling jets. The measured values of swirl number, S_1 at z/D = 0.1 for unconfined and confined jets are equal to 1.4 and 3, respectively. This increase in the swirl number value due to confinement clearly seen in the higher spreading of the jet as compared to unconfined jet (Figs. 4 (a) & (b)), which is in agreement with the Liang & Maxwothy [24] and Ceglia et al. [10].
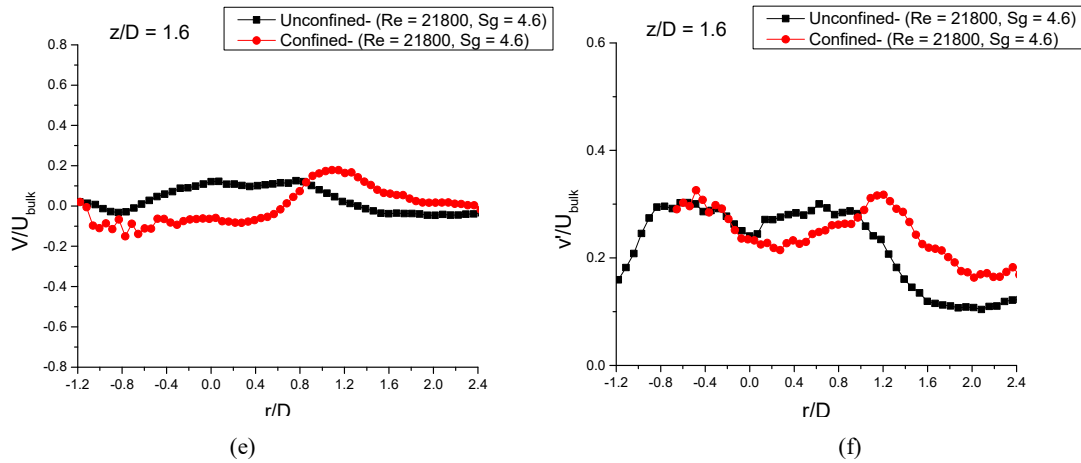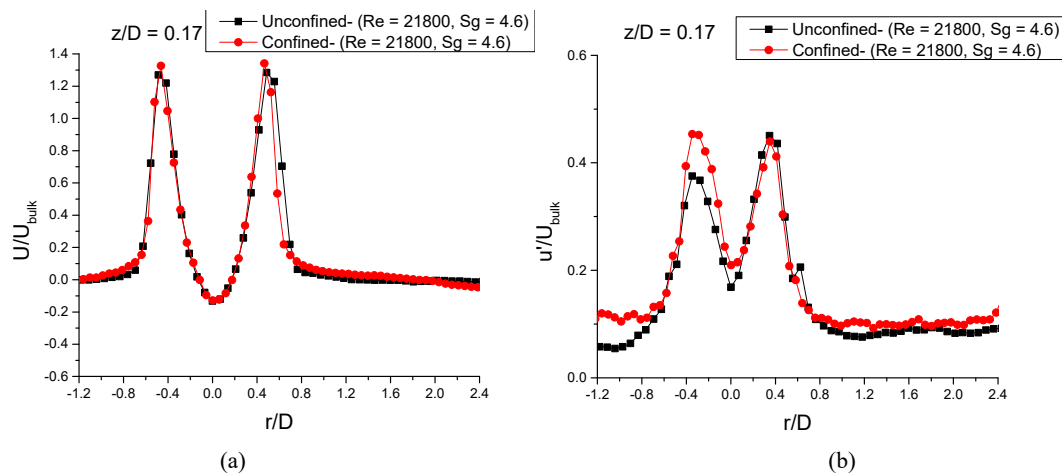

(a)

(b)

(c)

(d)

World Academy of Science, Engineering and Technology
International Journal of Mechanical and Mechatronics Engineering
Vol:11, No:2, 2017

(e)   (f)

Fig. 5 Normalized radial velocity components (a), (c) & (e) and its RMS fluctuations (b), (d) & (f) at Re = 21800 & S_g= 4.6 for both unconfined and confined flows

Normalized mean radial velocity component and its RMS fluctuations for both unconfined and confined flows are shown in Figs. 5 (a)-(f) for S_g = 4.6 and Re = 21800 at z/D = 0.17, 0.84 & 1.6. The radial velocity profiles show an anti-symmetric behavior near the nozzle exit for both unconfined and confined case are shown in Fig. 5 (a), in the region at which the velocity gradient decreases almost to zero, creating an area of low radial velocity in which the RMS fluctuation are intensified. In general the RMS fluctuations of radial velocity are high as compared to the bulk velocity, higher than the unconfined swirling jet case, in particular the central region of the jet at close distance to the nozzle exit and but similar values of radial velocity fluctuations in two localized edges of the jet at r/D $\cong$ 0.5 for both unconfined and confined case. Instead, the inner zone, corresponding to the region of negative axial velocity between the 0.4 < z / D <1.6 shows lower radial velocity fluctuations (Figs. 5 (d) & (f)). This behavior is also observed for the unconfined case.

Normalized mean axial velocity component and its RMS fluctuations for both unconfined and confined flows are shown in Figs. 6 (a)-(f) for S_g = 4.6 and Re = 21800 at z/D = 0.17, 0.84 & 1.6. The axial velocity profiles show a wake-like pattern and it is symmetric respect to the axis of the nozzle, we also noticed the presence of the flow reversal zone (or CRZ) which extends approximately from z/D = 0.08 up to z / D = 1.6 approximately for confined swirling jet (Fig. 4). The RMS fluctuation of axial velocity as shown in Figs. 6 (b), (d) & (f) presents the presence of the double shear layer for both unconfined and confined swirling jets respectively, one between the high-velocity region and the ambient fluid almost at rest in which fluctuations has larger values for confined case and the other with the flow reversal zone and low velocity region in which RMS fluctuation has lower values. At z/D = 1.6, the maximum values of the axial velocity fluctuations are achieved further away from the jet axis for the confined case as compared to unconfined case. This behavior is due to the spreading of the jet that influences the shape of the CRZ.
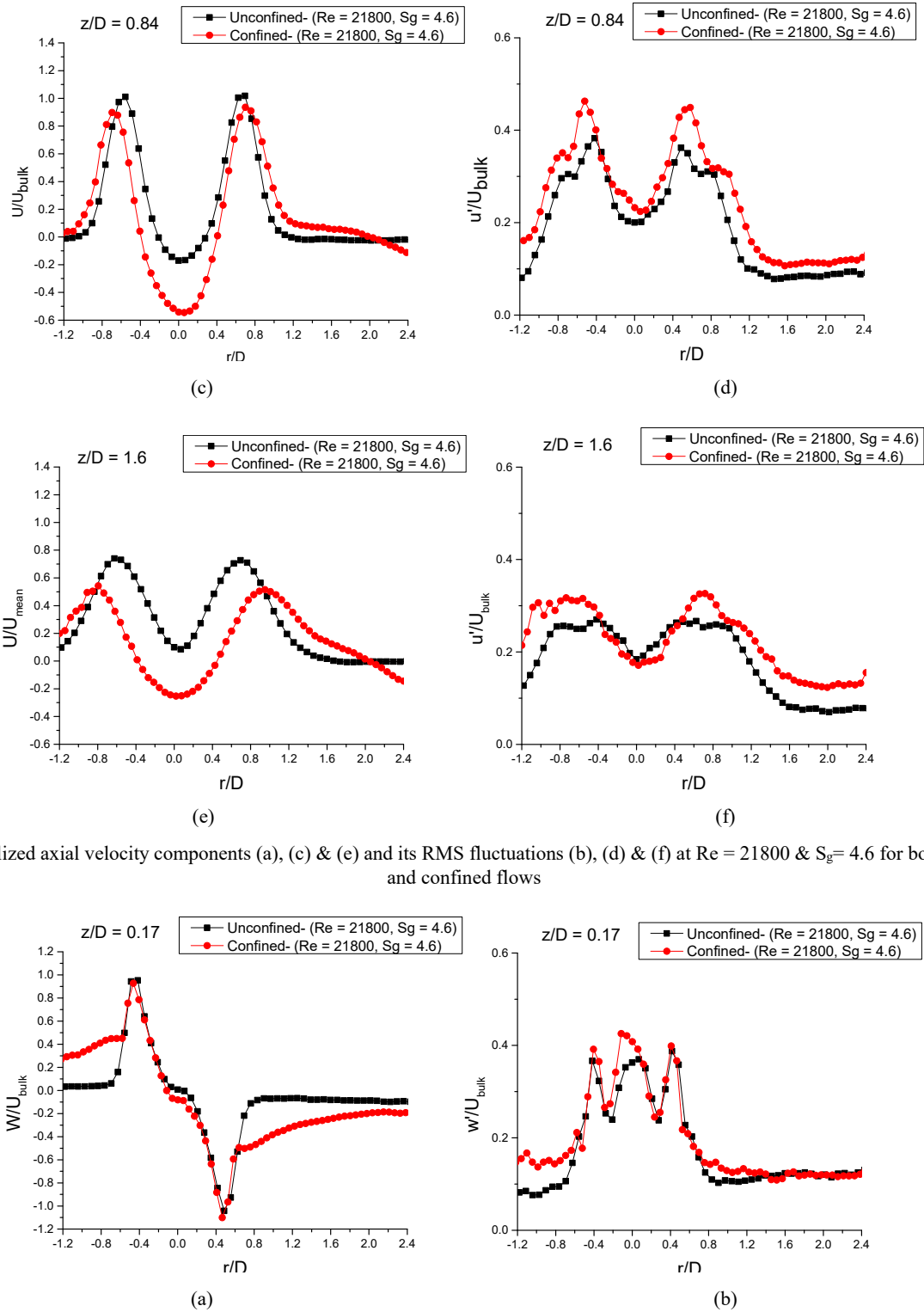

(a)   (b)

World Academy of Science, Engineering and Technology
International Journal of Mechanical and Mechatronics Engineering
Vol:11, No:2, 2017

Fig. 6 Normalized axial velocity components (a), (c) & (e) and its RMS fluctuations (b), (d) & (f) at Re = 21800 & Sg= 4.6 for both unconfined and confined flows
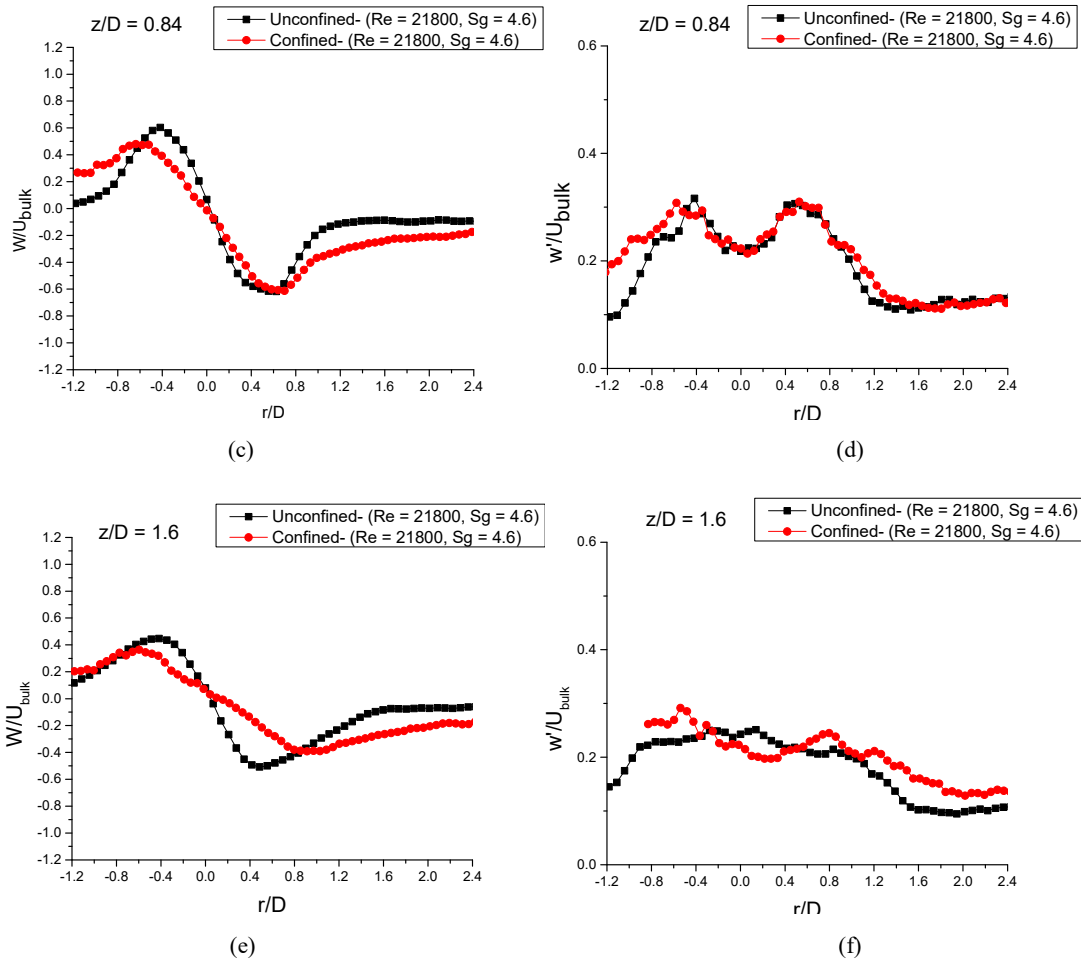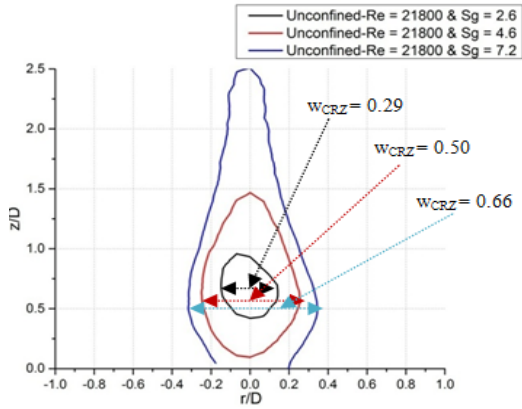
World Academy of Science, Engineering and Technology
International Journal of Mechanical and Mechatronics Engineering
Vol:11, No:2, 2017

Fig. 7 Normalized tangential velocity components (a), (c) & (e) and its RMS fluctuations (b), (d) & (f) at Re = 21800 & S_g= 4.6 for both unconfined and confined flows
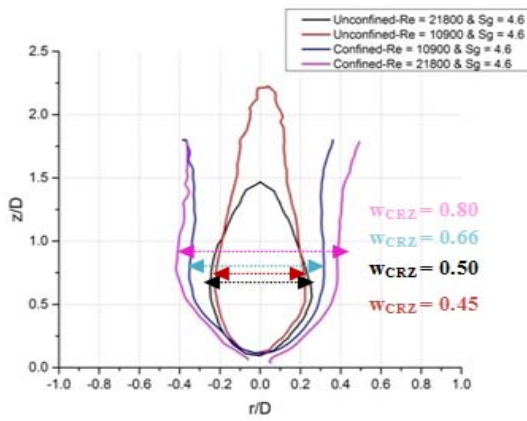
Normalized mean tangential velocity component and its RMS fluctuations for both unconfined and confined flows are shown in Figs. 7 (a)-(f) for S_g = 4.6 and Re = 21800 at z/D = 0.17, 0.84 & 1.6. The tangential velocity has an anti-symmetric profile with respect to the axis of the nozzle for both the cases as shown in Fig. 7 (a) with a zone where tangential velocity assumes values around zero at downstream position close to nozzle exit at r/D = 0, as can be seen from the profile z/D = 0.17, whose value is close to zero at axis. The RMS fluctuation of tangential velocity have more or less similar shape of radial velocity fluctuation but distribution in space is somewhat different, more intense fluctuations due to confinement in the central region near nozzle exit and two lateral areas in correspondence to the outer shear layer between the jet and the surrounding ambient, due to the creation of a low tangential velocity region in correspondence to the area in which reversal of flow has occurred at z/D = 0.17 as shown in Fig. 7 (a). Slightly downstream for z / D <1, is present circumscribed area in which the tangential velocity is close to zero corresponding to the recirculation zone (Fig. 6 (c)), where the standard deviation of tangential velocity shows the lowest values at z/D ≥ 0.3 (Figs. 7 (d) & (f)).

B. Effects of Reynolds Number

The better comparisons of recirculation zone shape for both unconfined and confined conditions, indicated by the contour line of zero axial velocity are shown in Figs. 8 (a) & (b). CRZ is enlarged with increasing swirl intensity for unconfined swirling jet as shown in Fig. 8 (a). CRZ further enlarged for confined case with increasing swirl number and Re. Increase in Reynolds number under confined isothermal conditions significantly increased the width of the recirculation zone as shown in Fig. 8 (b). Like our present case, Liang and Maxworthy [24] present two configurations where VB is present in the mean flow field. They suggested that two factors contribute to the enlargement of the swirling jet: turbulence and the displacement of the jet by the recirculation bubble. They found that at the same Re, the jet enlarged with the swirl number. The same observation made by Oberleithner et al. [13] who proposed that the recirculation bubble size increases with swirl number. Archer et al. [25] report that the width of the recirculation grows with confinement, moreover increasing the Reynolds number under isothermal condition significantly increased the strength of the recirculation zone. Our results qualitatively agreed with the previous studies in both unconfined and confined swirling jet.

World Academy of Science, Engineering and Technology
International Journal of Mechanical and Mechatronics Engineering
Vol:11, No:2, 2017

(a)

(b)

Fig. 8 Shape of the recirculation zone, defined by the contour line of zero axial velocity. (a) - For unconfined flow for same Re and different S_g, (b) - For both unconfined and confined flow with different Re at S_g = 4.6

C. POD Analysis

The POD analysis was performed for unconfined and confined swirling jet at S_g = 4.6 & Re = 21800, respectively. The energy distribution of the POD modes obtained as the ratio between the each eigen value and the sum of entire set of eigen values. The total energy fraction and cumulative energy distribution per POD modes for both measurements is shown in Figs. 9 (a) & (b). The energy contribution of first two modes is 12.4% for unconfined jet and 10.44% for confined jet (Fig. 9 (a)). For the confined case, the contribution of the first two modes are slightly less energetic as compared to unconfined jet, this difference may be induced by the simultaneous presence of CRZ and corner recirculation zone (CoRZ) present in confined case. Fig. 9 (b) shows the convergence of cumulative energy fraction of the POD modes towards 100% is relatively faster for unconfined swirling jet up-to mode 63 $i.e$ $\frac{Mode\ Number}{N} \cong 0.09$ approx after that become slower as compared to the confined swirling jet.
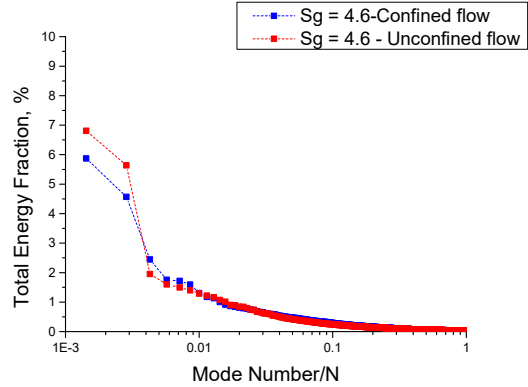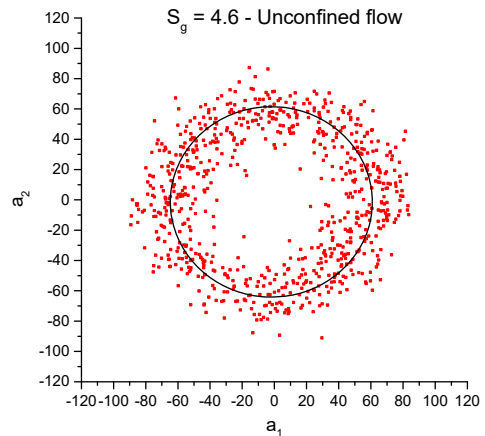

(a)
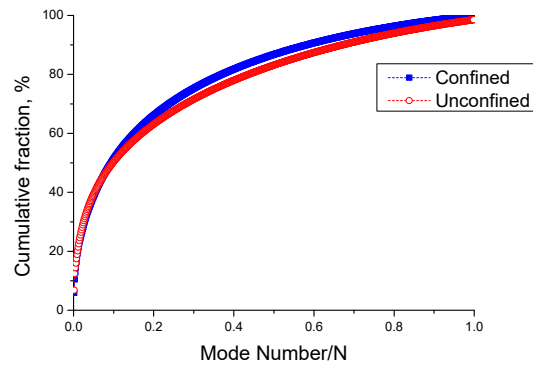
(b)

Fig. 9 (a) - Total energy distribution, (b) - Cumulative energy distribution per mode in strongly swirling flow i.e. S_g = 4.6 & Re = 21800 for both unconfined and confined in the longitudinal plane. The mode number is normalized with the number of snapshots (N)

The phase portraits of the corresponding amplitudes a_1 and a_2 for unconfined and confined swirling jet clearly show the existence of an oscillating behavior as shown in Figs. 10 (a) & (b). Oudheusden et al. [12] and Chong et al. [26] proposed to calculate the phase angle, $\theta(t) = \arctan\left(\frac{a_2(t)}{a_1(t)}\right)$, for each PIV snapshot with the corresponding time dependent POD mode coefficients a_1 and a_2 as given below.
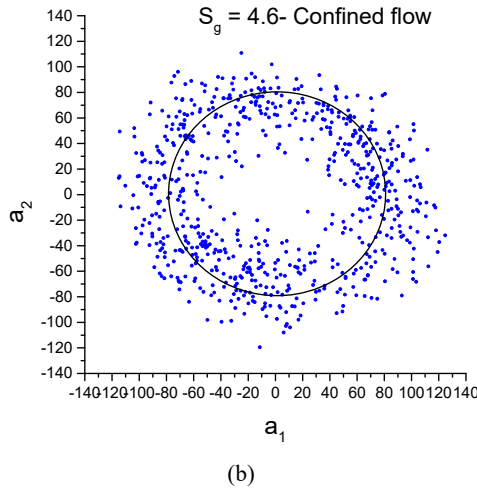

(a)

World Academy of Science, Engineering and Technology
International Journal of Mechanical and Mechatronics Engineering
Vol:11, No:2, 2017

(b)

Fig. 10 Phase portrait of mode coefficients a_1 and a_2 for (a) - unconfined swirling jet, (b) - confined swirling jet in the longitudinal plane, the solid line is a circular fit and similar to Lissajous figure
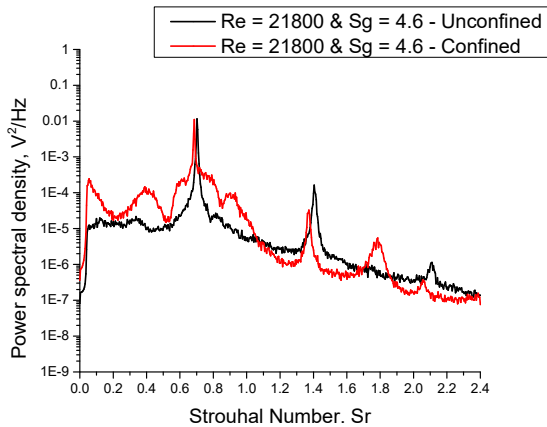

Fig. 11 Spectral analysis for unconfined and confined flow

The presence of a well-defined periodic signal is also characterized by acquiring the pressure fluctuations caused by the flow field by capacitive microphone. A spectral analysis according to the Bartlett method [29] and with a frequency resolution of 1 Hz was applied to the pressure signal to identify the PVC frequency. The precession of the vortex core is almost periodic and its trademark is clearly visible for both unconfined and confined swirling jet in the power spectra of pressure oscillation as shown in Fig. 11. The PVC is indicated by sharp peak in the spectra at frequency f_{PVC} = 175 Hz (Sr = $\frac{f_{PVC} D}{U_{bulk}}$= 0.70) for unconfined case and f_{PVC} = 171 Hz (Sr = 0.685) for confined case where the pulsation amplitude is observed to change rapidly by two orders of magnitude. The presence of a second harmonic at twice the precession frequency is also visible for both cases (Fig. 11).

Following the approach proposed by Oudheusden et al. [12], the 3D helical vortex structure is then reconstructed by using the minima of negative phase averaged swirl strength for unconfined (see Sharma et al. [27] for details) and confined swirling jet. Iso-surface of the 3D structure of swirl strength

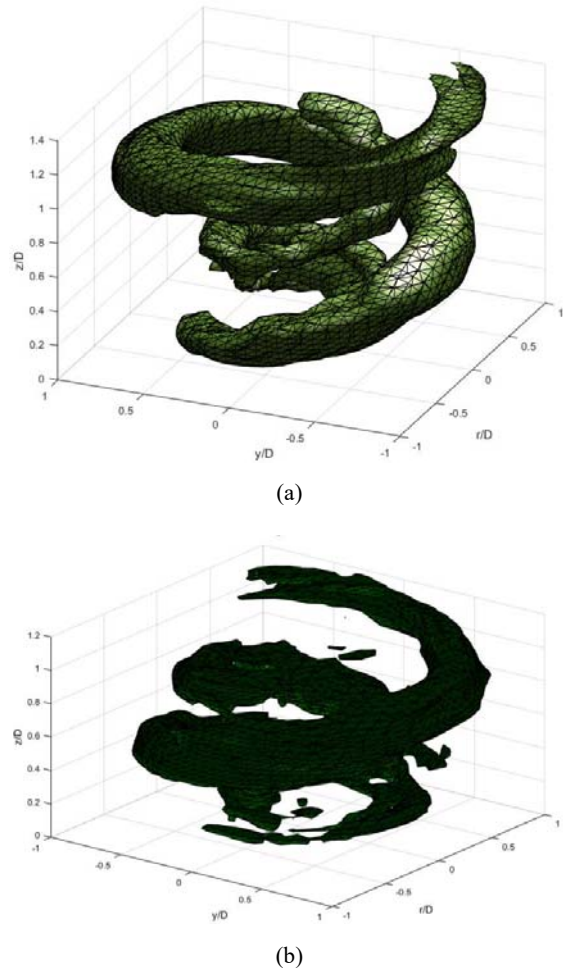for unconfined and confined swirling jet is shown in Figs. 12 (a) & (b).

(a)

(b)

Fig. 12 Iso-surface of swirl strength for S_g = 4.6 & Re = 21800. (a) - Unconfined swirling jet, (b) - Confined swirling jet

The two co-winding counter-rotating helical vortices appears to fade out at an axial location of approximately z/D = 1.2 for confined jet as compared to z/D = 1.5 for unconfined jet. It can be seen that the vortices are slightly suppressed due to confinement. A similar vortex structure was noticed experimentally by Markovich et al. [28].

VI. CONCLUSION

A 3C-2D PIV system was employed to characterize the unconfined and confined isothermal swirling jet associated with axial-plus-tangential entry type swirl generator. Detailed measurements were made for Re = 21800 and S_g = 4.6.Confinement effects on the flow field structure were investigated experimentally. The average velocity components and its RMS fluctuation of the highly swirling jet were used to analyze the behavior of the flow under unconfined and confined conditions. The flow field is influenced by the presence of VB in both the cases, with long and wide central recirculation region was noticed at the downstream position

World Academy of Science, Engineering and Technology
International Journal of Mechanical and Mechatronics Engineering
Vol:11, No:2, 2017

for confined case as compared to an unconfined case. Confinement increased the length of the recirculation zone (i.e. region of negative axial velocity, U≤0) and increased its width as compared to unconfined case for the same conditions. Increase in Reynolds number under confined isothermal conditions significantly increased the strength of the CRZ. The presence of the PVC instability was indicated by a sharp peak in the spectra of the acoustic pressure fluctuation acquired by a capacitive microphone. The energy contribution of first two modes is 12.4% for unconfined jet and 10.44% for confined jet, respectively. For the confined case, the contribution of the first two modes are slightly less energetic as compared to unconfined jet, this difference of the energy over the set of modes may be induced by the simultaneous presence of CRZ and corner recirculation zone (CoRZ) present in confined case. The time coefficients of the first two most energetic POD modes were used to reconstruct the phase of the oscillatory motion in the swirling flow. The 3D helical vortex structure obtained by using threshold value on the minima of negative phase averaged swirl strength and by assuming that the phase angle is equal to the angular rotation of the structure. It reveals the co-winding counter-rotating helical vortices originating in the inner and outer shear layer and this structure fade out at an axial location of approximately z/D = 1.5 for unconfined case and z/D = 1.2 for confined case.

REFERENCES

[1] K. Gupta, D.G. Lilley, N. Syred, Swirl Flows. Abacus Press, 1984.
[2] N. Syred, "A review of oscillation mechanisms and the role of the precessing vortex core (PVC) in swirl combustion systems," Progress in Energy and Combustion. Science, vol. 32(2), pp. 93–161, 2006.
[3] P. Billant, J.M. Chomaz, P. Huerre, "Experimental Study of Vortex Breakdown in Swirling Jets," Journal of Fluid Mechanics, Vol. 376, pp. 183–219, 1998.
[4] R. Chanaud, "Observations of oscillatory motion in certain swirling flows," J Fluid Mech 21:111–127, 1965.
[5] O. Lucca-Negro, T. O'Doherty, "Vortex breakdown," A review. Prog. Energy Combust. Sci. 27, 431, 2001.
[6] C.E. Cala, E.C.Fernandes, M.V. Heitor, S.I. Shtork, "Coherent structures in unsteady swirling jet flow," Exp Fluids 40:267–276, 2006.
[7] F. Martinelli, F. Cozzi, A. Coghe, "Phase-locked analysis of velocity fluctuations in a turbulent free swirling jet after vortex breakdown," Exp Fluids. 53:437-449, 2012.
[8] N. Syred, J.M. Beer, "Combustion in swirling flows: a review," Combustion and Flame, 23:143–201, 1974.
[9] A.E.E. Khalil, J.M Brooks, A.K. Gupta, "Impact of confinement on flowfield of swirl flow burners," Fuel 184, 1–9. 5, 2016.
[10] G. Ceglia, S. Discetti, A Ianiro, "Three-dimensional organization of the flow structure in a non-reactive model aero engine lean burn injection system," Exp ThermFluid Sci 52:164–173, 2014.
[11] M. Negri, F. Cozzi, S. Malavasi, "Self-synchronized phase averaging of PIV measurements in the base region of a rectangular cylinder," Meccanica 46: 423-435, 2010.
[12] B.W. van Oudheusden, F. Scarano, N.P. van Hinsberg, D.W. Watt, "Phase-resolved characterization of vortex shedding in the near wake of a square-section cylinder at incidence," Exp Fluids 39: 86-98, 2005.
[13] K. Oberleithner, M. Sieber, C.N. Nayeri, C.O. Paschereit, C Petz, H.C. Hege, "Three-dimensional coherent structures in a swirling jet undergoing vortex breakdown: stability analysis and empirical mode construction," J Fluid Mech 679:383-414, 2011.
[14] M. Stohr, R. Sadanandan, W. Meier, "Phase-resolved characterization of vortex-flame interaction in a turbulent swirl flame." Exp Fluids 51:1153-1167, 2011.
[15] H. Chen, D.L. Reuss, V. Sick, "On the use and interpretation of proper orthogonal decomposition of in-cylinder engine flows," Meas Sci Technol 23: 085302, 2012.
[16] J.L. Lumley, "The structure of inhomogeneous turbulence," In: Yaglom AM, Tatarski VI (eds) Atmospheric turbulence and wave propagation. Nauka, Moscow, 166-178, 1967.
[17] F. Cozzi, R. Sharma, A. Coghe, F. Arzuffi, "An experimental investigation on Isothermal free swirling jet," XXXVIII Meeting of the Italian Section of the Combustion Institute, 2015, Lecce, Italy.
[18] S.M. Soloff, R.J Adrian, Z.C Liu, "Distortion compensation for generalized stereoscopic particle image velocimetry," Meas. Sci. Technol.8:1441-1454, 1997.
[19] N.A. Chigier, A. Chervinsky A, "Experimental investigation of swirling vortex motion in jets," J Appl Mech 34:443–451, 1967.
[20] N. Rajaratnam, Turbulent Jets. Elsevier, Amsterdam, 1976.
[21] T.C. Claypole, N. Syred, "The Effect of Swirl Burner Aerodynamics on NOx Formation," International Symposium on Combustion, 1981, 18, 81–89.
[22] G. Berkooz, P. Holmes, J.L. Lumley, "The proper orthogonal decomposition in the analysis of turbulent flows," Annu Rev Fluid Mech 25:539-575, 1993.
[23] L. Sirovich, "Turbulence and the dynamics of coherent structures," Quart Appl Math 45: 561-590, 1987.
[24] H. Liang, T. Maxworthy, "An experiment investigation of swirling jets," J Fluid Mech 525:115–159, 2005.
[25] S. Archer, A.K. Gupta, "The role of confinement on flow dynamics under fuel lean combustion," In: 2nd international energy conversion engineering conference, 16–19 August, Providence, RI. Paper#AIAA-5617, 2004.
[26] P. Chong, W. Hongping, W. Jinjun, "Phase identification of quasi-periodic flow measured by particle image velocimetry with a low sampling rate," Measurement Science and Technology 24:055305, 2013.
[27] R. Sharma, F. Cozzi, A. Coghe, "Phase-averaged characterization of turbulent isothermal free swirling jet after vortex breakdown," Proc.18th International Symposium on the Application of Laser and Imaging Techniques to Fluid Mechanics, 2016, Lisbon, Portugal.
[28] D.M Markovich, S.S Abdurakipov, L.M Chikishev, "Comparative analysis of low- and high swirl confined flames and jets by proper orthogonal and dynamic mode decompositions," Phys Fluids 26:065109, 2014.
[29] G. John, P. Dimitris, G. Manolakis, Digital signal processing (3rd ed.): principles, algorithms, and applications, Prentice-Hall, NJ, USA, 1996.
[30] K. E. Meyer, D. Cavar, J. M. Pedersen, "POD as tool for comparison of PIV and LES data," 7th International Symposium on Particle Image Velocimetry, 2007, Rome, Italy.